ACS APPLIED MATERIALS & INTERFACES

Research Article

www.acsami.org

Flexible Transparent Metal/Polymer Composite Materials Based on Optical Resonant Laminate Structures

Sudarshan Narayanan, Jihoon Choi,† Lisa Porter, and Michael R. Bockstaller*

Department of Materials Science and Engineering, Carnegie Mellon University, 5000 Forbes Avenue, Pittsburgh, Pennsylvania 15213, United States

ABSTRACT: Suitable design of periodic metal/polymer composite materials is shown to facilitate resonant tunneling of light at absorbing wavelengths and to provide a means to significantly reduce optical absorption losses in polymer-based metallodielectric composite structures. The conditions for resonant tunneling are established based on the concept of "photonic band edge alignment" in 1D-periodic systems. For the particular case of a four-layer gold/polystyrene laminate structure, it is shown that the matching of the lower band edge of the 1D-periodic structure with the plasma frequency of the metal component facilitates the increase of optical transmission by about 500% as compared to monolithic film structures of equal total thickness. The effect of sheet thickness on the optical properties of thin metal films is determined and shown to be an important prerequisite for the reliable prediction of resonant metallodielectric structures. The resonant 1D-periodic metal/polymer heterostructures are shown to retain the flexural stability of the polymer matrix and thus could find application as flexible transparent conductors in areas such as "plastic electronics".

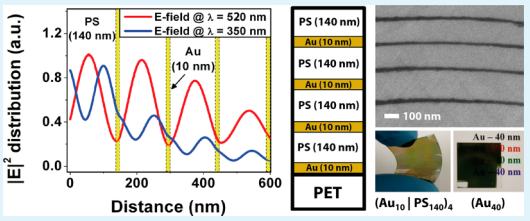

KEYWORDS: *photonic crystal, composite, transparent conductor, plastic electronics, thin metal film*

INTRODUCTION

Metallodielectric/polymer-matrix composite materials have received attention as a material platform for applications ranging from broadband power limiters for electromagnetic shielding to antistatic coatings and optical materials.[1−3] A general drawback associated with the addition of metals to polymer matrices is the increase of absorption that—in most circumstances—prevents the application of metal/polymer composite materials in areas where optical transparency is required. The strong absorption of metals arises due to fully occupied d-states in conjunction with the high free electron density close to the metals' Fermi levels, thus giving rise to interband and plasma absorption of incident electromagnetic waves.[4] The pronounced optical absorption of metals limits the distance that light (or other electromagnetic waves) of practical wavelengths can travel through a metal without incurring significant loss. The latter is often described in terms of the "skin depth" δ that corresponds to the distance along which the intensity of the wave $|E|^2$ decreases to $1/e$ of its value at the surface (where e denotes the Euler number). The small skin depth ($\delta \cong 20-40$ nm) of noble metals such as gold or silver in the visible wavelength range thus limits the application of metallic elements to ultrathin films if optical transparency is to be retained. An elegant approach to reduce optical losses in metal film structures was presented by Scalora and co-workers who demonstrated that the transmittance of laminated metallodielectric structures can be increased by several orders of magnitude as compared to monolithic metal film structures by taking advantage of a phenomenon called "optical resonant tunneling".[5,6] The latter refers to the effect of a suitably engineered periodic grating structure to redistribute the electric field of an incident electromagnetic wave such that at absorbing frequencies the field is concentrated within the nonabsorbing dielectric component while being depleted from the absorbing metal regions. As a consequence, light traversing the optically resonant structure experiences reduced absorption.

To date, the application of resonant tunneling to enhance the transmittance of metal-hybrid structures has focused on ceramic/metal (MgF_2/Ag) structures that allow for particularly efficient tunneling due to the favorable mismatch of the dielectric constants of the respective constituents (see discussion below). However, the brittle mechanical characteristics of ceramics in conjunction with the (often) weak interfacial bonding render ceramic/metal composite materials sensitive to mechanical damage or thermal-induced delamination that limit the application of ceramic/metal laminate structures.[7] In this contribution, we establish "design criteria" for the fabrication of optically resonant polymer/metal laminate structures and we demonstrate the fabrication of metal/polymer composite materials with 5-fold increase of optical transparency (as compared to the respective monolithic structures) that retain the mechanical flexibility and robustness that is characteristic of polymer materials. The excellent electron conductivity of laminated polymer/metal hybrid structures that is imparted by the continuous metal component could render the resulting "transparent metallodielectric nanocomposites" a platform for innovative material technologies in areas such as plastic electronics, power limiting, or

Received: December 21, 2012
Accepted: April 23, 2013
Published: April 23, 2013

thermo-photovoltaics for energy-recycling.[8−12] The structure of this article is as follows: First, we provide a brief review of the optical properties of 1D-periodic metallodielectric structures and establish the design parameters for optical resonant polymer/metal composite structures. Subsequently the fabrication of near-transparent polystyrene/gold laminate structures will be demonstrated and the optical properties evaluated against model calculations.

RESULTS AND DISCUSSION

A. Design of Transparent Metal/Polymer Optically Resonant Structures. The material system in our study consists of a lamellar stack of gold (Au) and polystyrene (PS) that were chosen because of the following property characteristics: PS (molecular weight M_n = 300 000 g/mol) is a transparent amorphous polymer with high softening temperature ($T_g \cong 110$ °C) and thus mechanically robust over a wide range of operating temperatures.[13−16] Polystyrene also has been shown to exhibit good wetability by metals such as Au or Ag (a key prerequisite for the deposition of thin, uniform films). Gold was chosen as a metal due to its chemical inertness and its good ductility that supports the flexural stability of polymer/metal laminate structures.[17,18] For the following discussion laminate structures will be abbreviated as $(Au_x|PS_y)_N$ where x and y represent the thickness (nm) of the Au and PS layer, respectively, and N represents the number of lamellar repeats. To identify suitable architectures for $(Au_x|PS_y)_N$ laminate structures that facilitate maximum tunneling efficiency, the transmission spectra as well as the electric field distribution of 1D-periodic metal-dielectric structures were calculated using the well-established transfer matrix method (TMM).[19] The primary prerequisite for enhanced optical transmission is that—at the absorbing wavelength—the electric field is concentrated within the transparent (polymer) layer. If the absorption of metals is dominated by free carrier excitation (approximately correct for noble metals), then the wavelength corresponding to the characteristic plasma absorption frequency ω_P should be chosen as a reference to minimize absorption (see discussion below). For example, Figure 1a depicts the electric field intensity distribution in an optimized metal−polymer stack comprised of four double layers of gold and PS $(Au_{10}|PS_{140})_4$ with layer thicknesses d_{Au} = 10 nm and d_{PS} = 140 nm, respectively. The figure reveals that at the absorption wavelength $\lambda = \lambda_P \cong 520$ nm the field intensity is concentrated within the PS layers. For this resonant condition the energy loss is significantly reduced as compared to an off-resonant condition (shown in the figure is the field distribution for λ = 350 nm)—the reduced energy loss is confirmed by the increase of $|E|^2$ of the transmitted wave for $\lambda = \lambda_P$. The comparison with the calculated field intensity $|E|^2$ of a monolithic film structure of equal overall thickness d_{Au} = 40 nm (depicted in Figure 1b) demonstrates the significant increase of transmittance at the plasma frequency of gold as compared to the monolithic film architecture.[20]

An alternative but useful approach to determine "optimum" film geometries is based on the analysis of the photonic band structure of the corresponding periodic metal/polymer stack. Because a photonic band gap in lamellar structures can be shown to arise as a consequence of the divergence of the electric field distribution at the band edges (with the field being concentrated in the high (low) refractive index layer at the lower (upper) band edge, respectively), the transmission condition is equivalent to the line-up of the plasma frequency

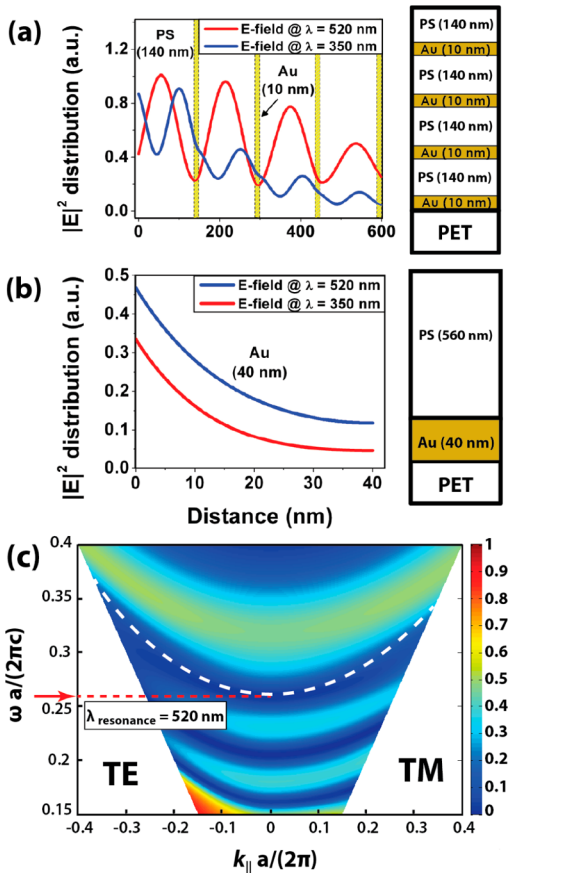

Figure 1. (a) Illustration of a $(Au_{10}|PS_{140})_4$ model resonant metallodielectric stack and calculated distribution of the electric field intensity $|E|^2$ that was determined by TMM (see text for more detail). The red curve corresponds to the calculation for the resonant condition λ = 520 nm (corresponding to the plasma wavelength of gold), and the blue curve, to off-resonant condition λ = 350 nm. For λ = 520 nm, the electric field is concentrated within the transparent PS-layer. (b) Illustration and calculated distribution of the electric field intensity $|E|^2$ of a monolithic gold film with thickness d_{Au} = 40 nm demonstrating rapid decay of the electric field. (c) Calculated frequency dependence of reflectivity for TE and TM polarization for a $(Au_{10}|PS_{140})_4$ metallodielectric stack. The simulation assumes optical constants of bulk gold. ω denotes the radial frequency, c is the vacuum speed of light, a denotes the lamellar repeat, and $k_\parallel$ is the parallel component of the wavevector with respect to the layer orientation. The reflectivity of normal incidence corresponds to $k_\parallel$ = 0. White lines indicate the location of the approximate location of the band gap (estimated for an infinite stack); the red arrow indicates the frequency of the lower band edge at $k_\parallel$ = 0.

with the *lower band edge* of the photonic structure (this is because the refractive index of metals approximately vanishes at the plasma frequency, and thus, the localization of the field in the transparent polymer layer is the greatest if the lower band edge matches the plasma frequency).[21] Figure 1c illustrates the optical reflection spectrum of the $(Au_{10}|PS_{140})_4$ structure calculated for an arbitrary angle of incidence for both TE and TM polarization along with the approximate position of the lower band edge (white dotted line) that was determined using TMM.[19,22] Note that at normal incidence (i.e., for $k_\parallel$ = 0) the lower band edge approximately coincides with the plasma frequency (indicated with the red arrow). Although the consideration of the "photonic crystal analogy" does not provide explicit new insights for transparent laminate

structures, it does highlight the relevance of the "band edge" in photonic structures and could provide a basis for the extension of the resonant tunneling approach to 2D and 3D periodic structures as well as to other forms of wave propagation (such as phonon propagation).[23,24]

To rationalize the particular choice of $(Au_{10}|PS_{140})_4$ in the present study, Figure 2 illustrates the effects of PS thickness

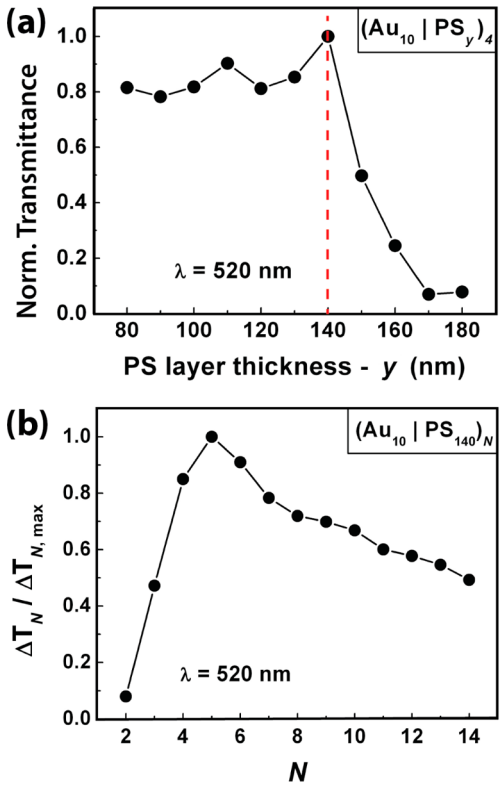

Figure 2. Dependence of tunneling efficiency on film architecture calculated using TMM. (a) Calculated transmission at λ = 520 nm of $(Au_{10}|PS_y)_4$ resonant structure (on glass substrate) as a function of the PS-layer thickness in the range y = 80 − 180 nm. Maximum transmission is predicted at y = 140 nm. (b) Dependence of quality factor for transmission enhancement $\Delta T_N = T_{stack,N} - T_{bulk,N}$ on the number of repeat units in $(Au_{10}|PS_{140})_N$ laminate structures (see text for more details). Maximum enhancement is observed at N = 5.

variation and the number of stacked lamellae on the film transmittance and tunneling efficiency of light (at λ = 520 nm) in the $(Au_{10}|PS_y)_4$ system. As depicted in Figure 2a, the maximum transmittance is expected for a thickness of the dielectric PS layer d_{PS} = 140 nm; however, the transmittance remains within 10% of the maximum value when the PS layer thickness is varied within the range 80 nm < d_{PS} < 145 nm. We note that in the above discussion the layer thickness of gold is fixed at d_{Au} = 10 nm. Although thinner films would be expected to facilitate higher transmittance (because the electric field concentration within the metal layer decreases with film thickness), eventually a decrease in electrical conductivity (as well as mechanical ductility) would be expected due to surface scattering.[24] Thus in reality a compromise has to be made to balance optical transmission and electric conductivity as well as mechanical ductility and stability; d_{Au} = 10 nm was determined to be an appropriate choice for the present system. The effect of layer nonuniformity on film transmittance was evaluated by simulating multilayer structures with variable thickness of the PS layer. For thickness variations within 5% of the average layer thickness $\langle d_{PS} \rangle$ = 140 nm, the transmittance was found to remain within 10% of its maximum value (the effect of random thickness fluctuations will be discussed more extensively in the context of Figure 5d below). Optical resonant tunneling in metal/polymer structures is thus reasonably tolerant against variations and imperfections of the layering process—an important feature for the application of the spin-coating approach to the fabrication of transparent metallodielectric composites.

To evaluate the number of periods corresponding to the maximum enhancement of light transmission, a quality factor was introduced as $\Delta T_N = T_{stack,N} - T_{bulk,N}$ where $T_{stack,N}$ and $T_{bulk,N}$ represent the transmittance of the $(Au_{10}|PS_{140})_N$ stack and the corresponding monolithic film of equal respective total thickness. ΔT_N thus provides a measure for the increase of transmittance due to resonant tunneling. As illustrated in Figure 2b, ΔT_N attains a maximum value at $N \cong 5$; however, it will remain within 10% of the maximum attainable transmission within the range N = 4−6. For reasons of practicality, N = 4 was chosen in the present study and thus the experimental demonstration of optical resonant metallodielectric structures will focus on the $(Au_{10}|PS_{140})_4$ architecture.

B. Fabrication and Characterization of Optically Resonant Polymer/Metal Hybrids. Metal/polymer stacks were prepared by alternating evaporation and spin-coating of Au and PS layers, respectively, on poly(ethylene terephthalate) (PET) substrates. PET was chosen as a substrate because of its optical transparency in the visible range as well as mechanical flexibility and toughness. Characterization of the film microstructure was performed by scanning (SEM) and transmission (TEM) electron imaging of cross-sectioned films. Figure 3

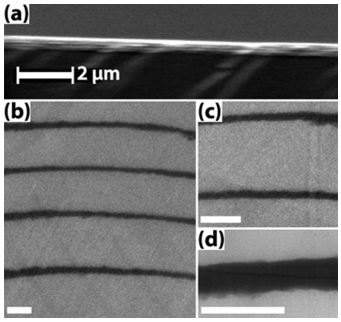

Figure 3. Electron microscopy analysis of film microstructure. (a) Cross-sectional SEM image of an Au/PS stack deposited on a glass substrate. (b−d) Cross-sectional TEM images of the stack prepared on a PET sheet, at different magnifications (substrate location is along the lower edge of micrographs). High magnification (d) reveals partial diffusion of gold into PS layers. Minor tilt misorientation of sectioned samples gives rise to distortions of the layer thickness. The scale bar is 100 nm.

depicts representative SEM (Figure 3a) and TEM (Figure 3b−d) images of a typical $(Au_{10}|PS_{140})_4$ stack, demonstrating the uniform structure and layer dimensions of the PS/Au model system (the substrate orientation is along the lower edges of the images shown in Figure 3b−d). We note that the precise thickness of the Au layer cannot be determined from cross-sectional TEM because of the potential mechanical distortion during sectioning. Rather, the thickness of the gold layers was determined in situ by a quartz crystal microbalance during

evaporation and independently verified by ellipsometry (results not shown here).

A minor asymmetry of the evaporated Au films (with respect to the substrate orientation) can be discerned from higher magnification micrographs (see Figure 3d) that is attributed to the partial diffusion of Au into the surface region of PS layers during the early stages of metal deposition. While it is possible to account for the effect of metal/polymer interdiffusion on the film optical properties, we found the diffusion lengths to be within a few nanometers (i.e., much smaller than the wavelength of light) and thus the effect of interdiffusion on optical properties is assumed to be negligible. A comment should be made regarding the effect of film thickness on the optical properties of the gold layer. As the thickness of the metal layer is decreased below a critical threshold value that is of the order of the electron mean free path l (for gold $l \cong 30$ nm), surface scattering events are expected to alter the dielectric properties (and thus the associated optical constants) of the metal film.[26] The implications of spatial confinement on the optical properties of metals are well-understood for the case of spherical nanocrystals for which it was shown that—within the free electron approximation—the effect of surface scattering on the dielectric constant of metals can be approximately accounted for by the introduction of additional damping terms in the Drude–Lorentz–Sommerfeld model.[25] In this case, the effect of spatial confinement is primarily on the imaginary component of the dielectric constant $\varepsilon_2 = 2nk$ (where n and k correspond to the real and imaginary part of the refractive index, respectively) such that $\varepsilon_2 \sim R^{-1}$ (with R denoting the particle radius).[23] In contrast to spherical systems, little information is available regarding the effect of spatial confinement on the optical constants in thin metal films. To the authors' knowledge, the first experimental studies on the effect of film thickness on the optical constants of metals are due to Krautkrämer and co-workers as well as Malé and co-workers who systematically evaluated the effect of film thickness on the optical constants of thin films of gold and silver.[27,28] A compilation of studies on the optical properties of thin metal films is provided in more recent reviews by Heavens.[29,30] The conclusion of these previous studies is that a significant reduction of the films' (complex) refractive index is expected for film thicknesses below 20 nm in the case of Au (and similarly for other metals such as Ag, Cu, Pt, and Pd). Since for the present $(Au_{10}|PS_{140})_4$ system, the thickness of the gold layers is significantly below the electron mean free path (and since for 10 nm layer thickness no experimental data is available in the wavelength range of interest), the optical constants n and k were determined experimentally to facilitate proper modeling of the films' optical response. Optical constants were measured for a series of gold films (deposited on glass) using variable-angle spectroscopic ellipsometry (VASE). Figure 4 summarizes the results for n and k for a range of tested film thicknesses d_{Au} = 5, 10, and 20 nm.

In agreement with previous reports, the optical constants of Au are found to sensitively depend on the films' thickness. While for thickness d_{Au} = 20 nm, the optical constants are close to bulk values (red line in Figure 4), both the real and imaginary parts of the refractive index differ markedly for smaller film thicknesses. Similar to spherical nanocrystal systems, the observed trend of n and k with d_{Au} is consistent with an increase of ε_2 with decreasing film thickness; however, no simple proportionality relation as for spherical particle systems could be established.[31] Within the range of

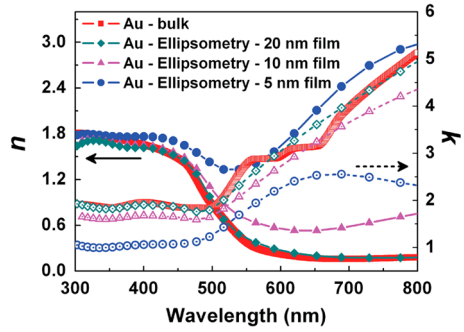

Figure 4. Comparison of the real part (n, solid lines) and imaginary part (k, dotted lines) of the refractive index of gold films of thickness d_{Au} = 5 (blue), 10 (purple), and 20 nm (green) that were determined by VASE. The figure reveals that for 20 nm film thickness the optical constants correspond approximately to those of bulk gold (red); for films with thickness d_{Au} < 20 nm a pronounced deviation from bulk values is observed (see text for more details).

experimental wavelengths ($300 < \lambda < 800$ nm), the values of n and k were found to be adequately represented by a seventh order polynomial—the details of the polynomials describing the optical constants of Au thin films (within the wavelength range $300 < \lambda < 800$ nm) are provided in the Materials and Methods section. For the simulation of film transmittance, experimental values corresponding to a film thickness d_{Au} = 10 nm were assumed.

Figure 5a and b shows pictures of the monolithic Au film (d_{Au} = 40 nm, Figure 5a) and the corresponding metallodielectric $(Au_{10}|PS_{140})_4$ resonant structure (Figure 5b) on a PET substrate demonstrating the significant increase in transparency facilitated by resonant tunneling. The optical properties as well as film structure were retained during repeated flexural deformation of the PET substrate (see Figure 5c) thus illustrating the potential applicability of polymer-based metallodielectric resonant structures as, for example, transparent flexible conductive substrates or electrodes in polymer electronics.[32] A comment should be made regarding the origin of the flexible character of a PS-based laminate structure (since PS is commonly known to be a brittle polymer glass at room temperature). We interpret the flexural stability of the PS laminate structure to be a consequence of the thin film configuration that allows for lateral deformation of the material during stress application on the films (for example, during bending of the film). The resulting *plane-stress* condition leads to an increase in the materials' toughness and is responsible for the markedly different deformation characteristics in thin films as compared to bulk materials.[33−36]

To quantify the increase in transmission that is facilitated by resonant tunneling, the film absorption was determined using optical spectroscopy. Figure 5d confirms the increase in optical transmission at λ = 520 nm by approximately 500% as compared to the monolithic film. This increase in transmission is consistent with the predicted increase of the field amplitude $|E|^2$ in the resonant structure that is depicted in Figure 1a and b. The experimental transmission data of the resonant structure (red line) is in excellent agreement with the predicted values based on the TMM simulation (assuming optical constants corresponding to the experimental data of thin films reported in Figure 4), thus providing further evidence for the tunneling mechanism. Note that the agreement between the experimental and calculated values sensitively depends on the proper choice

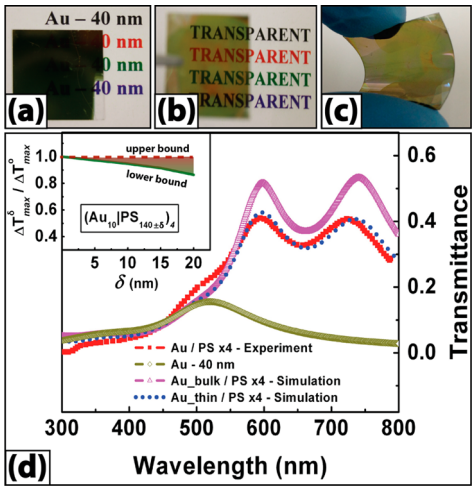

Figure 5. Optical characterization of $(Au_{10}|PS_{140})_4$ resonant structures. (a) Picture of monolithic Au film (d_{Au} = 40 nm) deposited on PET substrate. (b) Picture of $(Au_{10}|PS_{140})_4$ laminate film deposited onto PET substrate revealing the pronounced increase in transparency as compared to the monolithic film (a). (c) Image of the $(Au_{10}|PS_{140})_4$ resonant structure demonstrating film flexibility. (d) Optical transmission spectra of $(Au_{10}|PS_{140})_4$ (red curve) and monolithic Au film (d_{Au} = 40 nm, gold curve) revealing approximately 500% increase of transmission at λ = 520 nm for the resonant structure. The dotted blue line corresponds to TMM prediction of transmission assuming optical constants corresponding to d_{Au} = 10 nm film thickness (data shown in Figure 4). The dotted purple line corresponds to simulation assuming bulk optical constants of gold. The inset shows the effect of random thickness variations of the PS layer for a multilayered structure with N = 4 on the normalized maximum transmittance $\Delta T^{\delta}_{max}/\Delta T^{0}_{max}$ (where ΔT^{0}_{max} is the maximum transmittance of the uniform structure relative to that of the corresponding monolithic Au film). For each thickness variation δ, T_{max} was determined from the particular realization of a four layer stack $(Au_{10}|PS_{140\pm\delta})_4$ corresponding to minimum film transmittance and the constraint $\langle d_{PS}\rangle$ = 140 nm.

of optical constants according to the film thickness. This is illustrated by comparison with the calculated transmission values assuming bulk values for the optical constants of gold (pink curve) that significantly overestimate attainable film transparencies.[37] We note that the excellent agreement between calculations for an idealized uniform geometry and the experimental system that necessarily includes minor variability of layer thickness due to the film fabrication procedure is an indicator for the robustness of the optical resonant tunneling effect with regard to structural defects.

To understand the effect of random PS-layer thickness variation on the films' optical properties, the transmission spectra of different realizations of four-layer stacks were calculated assuming a random fluctuating thickness of each PS layer according to d_{PS} = 140 ± δ nm (where δ denotes the respective thickness variation) under the constraint of constant average layer thickness $\langle d_{PS}\rangle$ = 140 nm. The maximum reduction of the films' optical transmittance (and thus the lower bound for optical transmission) due to the nonuniformity of the PS layer thickness was subsequently determined by comparison of the maximum transmittance values of the ideal (uniform) stack with the corresponding four layer variable stack $(Au_{10}|PS_{140\pm\delta})_4$ that exhibits the lowest optical transmittance (of all possible configurations). The inset of Figure 5d depicts the effect of a random thickness variation (of the PS layer) on the films' maximum attainable transmittance and reveals that ΔT (or equivalently the lower bound of T_{max}) remains within 10% of the optimum value (that corresponds to the uniform reference structure) for thickness fluctuations up to δ = 10 nm. We expect this robustness of the optical resonant tunneling effect to greatly benefit the applicability of this approach for the fabrication of polymer/metal composite structures with reduced optical absorption since it enables the use of rapid processing techniques such as spin-coating for which minor variations in layer thickness can be expected.

CONCLUSION

Optical resonant tunneling in periodic metal/polymer composite structures provides a means to significantly reduce optical absorption losses in polymer-based metallodielectric composite structures while retaining the advantageous (mechanical) properties of the polymer matrix. For the particular case of a 1D-periodic (laminate) structure, it is shown that a suitable strategy for the design of resonant structures is to align the lower band edge of the 1D-periodic (photonic crystal) structure with the plasma absorption frequency of the metal component. For the particular case of gold/polystyrene laminate structures, an increase of the optical transmission by about 500% is realized by the appropriate design of a four-layer structure. The resulting flexible and (near) transparent polymer/metal composite structures could provide a robust material platform for the fabrication of flexible transparent conductors that play a central role in the development of "organic flexible electronics". We note that for the latter application it is not the "absolute transparency" but rather the ratio of transparency and resistance that is used as a metric to classify the performance of transparent conductors. The high conductivity that is imparted by the metal component (in our case the in-plane conductivity was determined to be $\sigma \cong 10^6$ 1/(Ω cm)) should benefit the application of resonant metal/polymer composite structures as transparent conductors. Furthermore, the sensitivity of resonant tunneling to variations in the optical properties of the constituents could render these material systems interesting for a range of responsive material applications in which a minor change to one of the layers gives rise to an amplified collective response of the stack. Strategies to further enhance the optical transparency of resonant metal/polymer composite structures should focus on the use of metals such as Ag with a plasma frequency outside the visible range. Furthermore, the self-assembly of polymer/nanoparticle composite systems into laminate structures could be explored as a more efficient and scalable fabrication methodology for resonant metal/polymer composite structures.[38−40]

MATERIALS AND METHODS

Materials. Polystyrene (PS) solution was prepared by dissolving 3 wt % of the polymer (M_n = 300 000 g/mol, molecular weight dispersity index $Đ$ = 1.15, Polymer Science, Inc.) in toluene. The solution was filtered using a 0.45 μm PTFE filter prior to use. Gold pellets obtained from Kurt. J. Lesker, Inc., were used for evaporation.

Sample Preparation. PS films were prepared by spin-coating the PS solutions for 30 s. The spin rate was varied between 1500 and 4000 rpm to arrive at a thickness of ∼140−150 nm, consistent with the thickness required as per simulations. The appropriate deposition conditions were determined by spin-casting films on silicon and subsequent evaluation of their thicknesses using ellipsometry and spectral reflectometry (Filmetrics). Au thin films were deposited using an electron-beam evaporation system (Thermionics, Inc.) at a rate of

Table 1. Fitting Parameters Used to Represent Optical Constants (n, k) for Gold Thin Films of Various Thicknesses[a]

	Au−5 nm		Au−10 nm		Au−20 nm	
parameter	n	k	n	k	n	k
p_1	1.396	1.617	0.866	2.015	0.6747	2.243
p_2	−0.039	1.756	−1.423	1.621	−1.755	1.781
p_3	1.948	0.370	0.907	1.205	0.980	1.37
p_4	0.863	−1.591	1.385	−0.849	1.553	−0.948
p_5	−1.652	−0.0232	−1.053	−0.336	−1.261	−0.353
p_6	−0.194	0.577	−0.378	0.373	−0.409	0.428
p_7	0.570	−0.165	0.449	−0.074	0.533	−0.089
p_8	−0.130	0.00539	−0.0907	0	−0.111	0
R^2 error	0.995	0.991	0.991	0.998	0.992	0.997

[a] λ is in nanometers.

0.5 Å/s under UHV conditions. The thicknesses of the Au films were 10 nm as determined by an in situ quartz crystal microbalance.

Optical Characterization. Transmission spectra were recorded using a spectroradiometer (Optronics OL 770 LED test measurement system). Variable-angle spectroscopic ellipsometry was performed using a VASE courtesy J. A. Woollam Co. Inc. To establish optical constants of Au as a function of film thickness, films of d_{Au} = 5, 10, and 20 nm thicknesses were prepared on glass substrates by e-beam evaporation. The optical constants n and k were adequately captured by a seventh order polynomial of the form

$$n(\text{or } k) = p_1 + p_2\lambda + p_3\lambda^2 + p_4\lambda^3 + p_5\lambda^4 + p_6\lambda^5 + p_7\lambda^6 + p_8\lambda^7 \quad (1)$$

Table 1 summarizes the respective fitting parameters for the different film configurations that were evaluated in the present study.

Electron Microscopy. Transmission electron imaging of sectioned film microstructures was performed using a JEOL 2000 FX electron microscope operated at 200 kV. Imaging was based on the amplitude and phase contrast, and images were recorded by a Gatan Orius SC600 high resolution camera. Prior to imaging films were sectioned at T = −120 °C using a Reichert Ultracut ultracryomicrotome. Scanning electron imaging was performed using a Philips XL-30 scanning electron microscope operating at 5 kV.

AUTHOR INFORMATION

Corresponding Author

*E-mail: bockstaller@cmu.edu.

Present Address

[†]J.C.: Department of Materials Science and Engineering, University of Pennsylvania, 3231 Walnut Street, Philadelphia, PA 19104-6272.

Notes

The authors declare no competing financial interest.

ACKNOWLEDGMENTS

This work was supported by the National Science Foundation (via grant DMR-1006473 and ECCS-0824188) as well as the Air Force Office for Scientific Research (via grant FA9550-09-1-0169). The authors also acknowledge the help of Andrea Donohue at J. A. Woollam Co., Inc., in evaluating the optical constants of gold thin films using VASE.

REFERENCES

(1) Bao, L.-R.; Wei, B.; Xiao, A. Y. Conductive Coating Formulations with Low Silver Content. *Proceedings of the 57th Electronic Components and Technology Conference*, Sparks, NV, May 29−Jun 21, 2007; pp 494−500.

(2) Bockstaller, M. R.; Thomas, E. L. *J. Phys. Chem. B* **2003**, *107*, 10017−10024.

(3) Bockstaller, M. R.; Thomas, E. L. *Phys. Rev. Lett.* **2004**, *93*, 166106.

(4) Fox, M. *Optical Properties of Solids*; Oxford University Press: New York, 2010; pp 143−154.

(5) Scalora, M.; Bloemer, M. J.; Pethel, A. S.; Dowling, J. P.; Bowden, C. M.; Manka, A. S. *J. Appl. Phys.* **1998**, *83*, 2377−2383.

(6) Scalora, M.; Bloemer, M. J.; Bowden, C. M. *Opt. Photonics News* **1999**, *10*, 24−27.

(7) Venkataraman, S. K.; Kohlstedt, D. L.; Gerberich, W. W. *Thin Solid Films* **1993**, *223*, 269−275.

(8) Kim, Y. S.; Park, J. H.; Choi, D. H.; Jang, H. S.; Lee, J. H.; Park, H. J.; Choi, J. I.; Ju, D. H.; Lee, J. Y.; Kim, D. *Appl. Surf. Sci.* **2007**, *254*, 1524−1527.

(9) Owens, D.; Fuentes-Hernandez, C.; Kippelen, B. *Thin Solid Films* **2009**, *517*, 2736−2741.

(10) Jakšić, Z.; Maksimović, M.; Sarajlić, M. *J. Opt. A: Pure Appl. Opt.* **2005**, *7*, 51−55.

(11) Vincenti, M. A.; Trevisi, S.; De Sario, M.; Petruzzelli, V.; D'Orazio, A.; Prudenzano, F.; Cioffi, N.; de Ceglia, D.; Scalora, M. *J. Appl. Phys.* **2008**, *103*, 064507 ff.

(12) Lin, S.-Y.; Fleming, J. G.; Moreno, J. A. *Photonic Crystals for Enhancing Thermophotovoltaic Energy Conversion*; Technical Report for the United States Department of Energy; Sandia National Laboratories: Albuquerque, NM, March 2003; pp 1−35, SAND2003-0845.

(13) The particular molecular weight of PS was chosen because of its fortuitous combination of film forming characteristics and fracture toughness of thin films. The latter has been shown to sensitively depend on chain entanglement that is expected to increase with increasing molecular weight. For more information on the subject of toughness in polymer materials, the reader is referred to refs 14−16.

(14) Choi, J.; Hui, C. M.; Pietrasik, J.; Dong, H. C.; Matyjaszewski, K.; Bockstaller, M. R. *Soft Matter* **2012**, *8*, 4072−4082.

(15) Graessley, W. W. *Adv. Polym. Sci.* **1974**, *16*, 1−179.

(16) Kramer, E. J. *Adv. Polym. Sci.* **1983**, *52*−*3*, 1−56.

(17) Lee, L. H. *Fundamentals of Adhesion*; Springer: New York, 1991; pp 50−63.

(18) Lopes, W. A.; Jaeger, H. M. *Nature* **2001**, *414*, 735−738.

(19) Born, M.; Wolf, E.; Bhatia, A. B.; Clemmow, P. C.; Gabor, D.; Stokes, A. R.; Taylor, A. M.; Wayman, P. A.; Wilcock, W. L. *Principles of Optics: Electromagnetic Theory of Propagation, Interference and Diffraction of Light*; Cambridge University Press: Cambridge, U.K., 2000.

(20) In the particular sample configuration discussed here, the top layer was chosen to be PS—this choice was based on mechanical stability considerations rather than the optical properties associated with this particular arrangement. Simulations show that for the present $(Au_{10}|PS_{140})_4$/substrate combination the optical properties are only weakly affected by the sequence of the stack.

(21) Joannopoulos, J. D.; Johnson, S. G.; Winn, J. N.; Meade, R. D. *Photonic Crystals: Molding the Flow of Light*, Second ed.; Princeton University Press: Princeton, NJ, 2008.

(22) In Figure 1c, TE (TM) correspond to the magnetic (electric) field being normal to the layer orientation. Note that for normal incidence both polarizations are equivalent.
(23) Gorishnyy, T.; Ullal, C.; Maldovan, M.; Fytas, G.; Thomas, E. *Phys. Rev. Lett.* **2005**, *94*, 115501 ff.
(24) Voudouris, P.; Choi, J.; Gomopoulos, N.; Sainidou, R.; Dong, H.; Matyjaszewski, K.; Bockstaller, M. R.; Fytas, G. *ACS Nano* **2011**, *5*, 5746−5754.
(25) Cottey, A. A. *Thin Solid Films* **1968**, *1*, 297−307.
(26) Kreibig, U.; Vollmer, M. *Optical properties of metal clusters*; Springer: New York, 1995.
(27) Krautkrämer, J. *Ann. Phys.* **1938**, *424*, 537−576.
(28) Malé, D.; Rouard, P. *J. Phys. Radium* **1953**, *14*, 584−587.
(29) Heavens, O. S. *Optical properties of thin solid films*; Butterworths Scientific: London, 1955.
(30) Heavens, O. S. *Rep. Prog. Phys.* **1960**, *23*, 1 ff.
(31) We note that the present data set is not sufficient to allow for quantitative comparisons of the confinement effect in spherical and planar metallic systems.
(32) Flexural deformation testing of laminated films consisted of repeated bending of films to a limiting curvature of $\kappa \sim 2$ cm^{-1}.
(33) Broek, D. *Elementary Engineering Fracture Mechanics*; Kluwer Academic Publishers: Hingham, MA, 1986.
(34) Choi, J.; Dong, H.; Matyjaszewski, K.; Bockstaller, M. R. *J. Am. Chem. Soc.* **2010**, *132*, 12537−12539.
(35) We note that a second contribution to the polymers flexibility could relate to spatial confinement effects due to the thin film confinement of PS. However, since the film thickness exceeds significantly the polymer's radius of gyration, i.e. 140 nm > $R_{g,PS300K} \cong$ 30 nm (the polymer's radius of gyration was estimated based on values reported in ref 36), we expect confinement effects to be negligible in the presented system.
(36) Brandrup, J., Imergut, E. H., Eds. *Polymer Handbook*, 3rd ed.; Wiley: New York, 1989.
(37) Palik, E. D., Ed. *Handbook of Optical Constants of Solids*; Academic Press Handbook Series; Academic Press: New York, 1997.
(38) Krishnan, R. S.; Mackay, M. E.; Duxbury, P. M.; Pastor, A.; Hawker, C. J.; Van Horn, B.; Asokan, S.; Wong, M. S. *Nano Lett.* **2007**, *7*, 484−489.
(39) Bockstaller, M.; Kolb, R.; Thomas, E. L. *Adv. Mater.* **2001**, *13*, 1783−1786.
(40) Bockstaller, M. R.; Mickiewicz, R. A.; Thomas, E. L. *Adv. Mater.* **2005**, *17*, 1331−1349.